Delamination toughening in a low carbon microalloyed steel plate rolled in the dual-phase region

Shen, X. J.; Li, D. Z.; Tang, S.; Chen, J.; Fang, H.; Wang, G. D.

DOI
10.1016/j.msea.2019.138342

Publication date
2019

Document Version
Final published version

Published in
Materials Science and Engineering A

Materials Science & Engineering A 766 (2019) 138342

Contents lists available at ScienceDirect

Materials Science & Engineering A

journal homepage: www.elsevier.com/locate/msea

Delamination toughening in a low carbon microalloyed steel plate rolled in the dual-phase region

X.J. Shen[a,*], D.Z. Li[a], S. Tang[a,**], J. Chen[a], H. Fang[b,c], G.D. Wang[a]

[a] The State Key Laboratory of Rolling and Automation, Northeastern University, P. O. Box. 105, No. 11, Lane 3, Wenhua Road, HePing District, Shenyang, 110819, China
[b] Fundamental Aspects of Materials and Energy Group, Faculty of Applied Sciences, Delft University of Technology, Mekelweg 15, 2629 JB, Delft, the Netherlands
[c] Novel Aerospace Materials Group, Faculty of Aerospace Engineering, Delft University of Technology, Kluyverweg 1, 2629 HS, Delft, the Netherlands

ARTICLE INFO

Keywords:
Steel plates
Delamination toughening
Elongated and ultrafine-grained microstructure
Crystallographic texture

ABSTRACT

It is still a big challenge to obtain excellent low-temperature toughness for bulk steel materials. Delamination is an effective method to improve low-temperature toughness. In the present study, delamination toughening in a low carbon microalloyed steel plate with elongated and ultrafine-grained microstructure rolled in the dual-phase region has been investigated in detail. When toughness was measured along normal direction, the steel plate had a high upper shelf energy and no delamination occurred in the upper shelf region. A large delaminated crack parallel to rolling plane started to appear and changed the propagation path of main crack when testing temperature was lower than −60 °C. We find this kind of delamination induces a second upper shelf in the Charpy transition–temperature curve. The second upper shelf, reaching up to 300 J in the temperature range of −60 °C to −140 °C, results in excellent low-temperature toughness for the steel plate, and the ductile-brittle transition temperature is lowered to −157 °C. The developed steel plate also has high low-temperature toughness measured along transverse direction due to delamination. The effect factors on upper shelf energy, delamination mechanism and delamination toughening are discussed.

1. Introduction

Developing stronger and tougher steels is of great interests to metallurgists. It is well known that grain refinement is an effective and economical way to achieve such properties for steels [1–3]. However, achieving excellent low-temperature toughness is still a big challenge for bulk steel materials due to the limited degree of grain refinement [4–6]. Some studies show that delamination can contribute to low-temperature toughness. Kum et al. found the delaminated crack propagated along the layered boundary leaded to excellent toughness in a laminated composite that the ductile-brittle transition temperature (DBTT) was lower to −140 °C and high shelf energy was larger than 325 J [7]. Inoue et al. developed a fibrous and ultrafine-grained microstructure in a plain carbon steel with DBTT reduced from −45 °C to −165 °C [8]. The excellent toughness was mainly caused by delamination. The reason for the improved toughness by delamination is that delamination relaxes the stress at the crack tip so that crack is blunted. Thus, plastic deformation and ductile fracture are enhanced. This is called delamination toughening. Therefore, excellent low-temperature toughness can be achieved via delamination toughening for the bulk steels.

Applying rolling in ferrite region for steel plates, elongated and ultrafine-grained (EUG) microstructures can be obtained. High low-temperature toughness can be acquired, but the upper shelf energy is low in the Charpy transition–temperature curve, compared with their coarse-grained (CG) counterparts produced by the conventional thermo-mechanical controlled processing (TMCP) [9–11]. The low upper shelf energy means inferior toughness at room temperature. In our previous study, we found high upper shelf energy could be attained in the EUG steel plates rolled in the dual-phase region. Excellent low-temperature toughness was achieved by controlling microstructure and crystallographic texture [12].

However, the previous study only focused on the toughness measured along transverse direction (TD) where the impact load parallel to during Charpy impact testing. The toughness measured along normal direction (ND) has not been investigated. Zou et al. achieved a high upper shelf energy higher than 450 J via delamination toughening in a 0.05C-5.0Mn-0.5Si-1.4Ni-0.12V (mass%) steel plate when toughness was measured along ND [13]. Zhang et al. obtained a laminated dual-phase microstructure via adding 3% Al to a 5%Mn steel plate to obtain

* Corresponding author.,
** Corresponding author.
E-mail addresses: shenxinjun@ral.neu.edu.cn, shenxinjun2008@163.com (X.J. Shen), tangshuai@ral.neu.edu.cn (S. Tang).

https://doi.org/10.1016/j.msea.2019.138342
Received 25 July 2019; Accepted 27 August 2019
Available online 31 August 2019
0921-5093/

Table 1
Chemical composition of the EUG steel plate (mass%).

Fe	C	Si	Mn	P	S	Nb	V	Ti
Balance	0.10	0.32	1.5	0.015	0.003	0.04	0.06	0.015

elongated δ-ferrite grains during rolling so that high toughness was obtained via delamination toughness measured along ND [14,15]. Judging from the microstructure and crystallographic texture characters of the EUG steel plates, one can expect that the delamination will be pronounced when the impact load goes along ND. Therefore, excellent low-temperature toughness will be obtained via delamination toughening. In the present study, the effect of delamination on toughness measured along ND in a EUG low carbon microalloyed steel plate was investigated in detail.

2. Experimental procedure

In the present study, chemical composition of the EUG steel plate with a thickness of 12 mm is listed in Table 1. The EUG steel plate was prepared by the following two steps. First, a steel billet with a thickness of 140 mm was hot-rolled to 65 mm thickness, followed by water-quenching to room temperature. This water-quenched steel slab was then reheated up to 810 °C and held for 7200 s to homogenize the temperature. According to our previous work, the slab was held in the dual-phase region that the microstructure was composed of bainitic ferrite and a small amount of austenite [12]. Second, nine passes rolling was carried out using a Φ450 mm two-high reversible trail mill. The total reduction was 81.5% in thickness. Thus, a steel plate with a thickness of 12 mm was obtained. The rolling schedule is listed in Table 2. The starting rolling temperature was very close to the reheating temperature. To minimize the temperature dropping during rolling period of the EUG steel plate, a short interpass time about 5 s was controlled. The steel plate was held for 300 s in the furnace after the fourth and seventh passes to compensate the temperature dropping. The finishing rolling temperature was about 780 °C. Then the steel plate was water-cooled to 633 °C at a cooling rate of about 10 °C/s followed by air cooling to room temperature.

For comparison, a CG steel plate was prepared via TMCP under the same rolling schedule, and the holding thickness was 30 mm. The starting rolling temperature and finishing rolling temperature in rough rolling period were 1080 °C and 1034 °C, respectively. The starting rolling temperature and finishing rolling temperature in finishing rolling period were 855 °C and 810 °C, respectively. The interpass time was also about 5 s. Then the steel plate was water-cooled to about 610 °C at a cooling rate of about 10 °C/s followed by air cooling to room temperature.

Samples for microstructure observation were sectioned at quarter width of the EUG steel plate and CG steel plate, respectively. After mechanical polishing, the samples were etched with 4% Nital solution. The microstructures on longitudinal section at quarter thickness were examined using a ZEISS ULTRA 55 field emission scanning electron microscope (FE-SEM). Electron back-scattered diffraction (EBSD) analyses were performed to obtain the grain orientations, distributions of grain boundary misorientation angles and grain sizes of the EUG steel plate and CG steel plate at the quarter thickness on the longitudinal section. The samples for EBSD analyses were prepared by electropolishing. The scanning areas were 80 μm × 100 μm at a step size of 0.15 μm. EBSD analyses were carried out through this ZEISS ULTRA 55 FE-SEM equipped with an EBSD attachment (Oxford Instruments, INCA Crystal). The crystallographic textures were measured by a Bruker D8 Discover X-ray diffractometer (XRD) for both the EUG steel plate and CG steel plate on plane at the quarter thickness parallel to the rolling plane. The samples were also prepared by electropolishing.

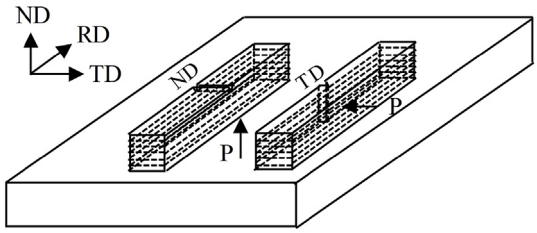

Fig. 1. Schematic diagram of the Charpy V-notch impact specimens in the EUG steel plate. P is the impact load during Charpy impact testing.

Toughness of the EUG steel plate was measured along ND in the temperature range from 0 °C to −196 °C. The Charpy V-notch impact specimens with 10 mm × 10 mm × 55 mm in size were machined along RD in the EUG steel plate, as shown in Fig. 1. We also measured the toughness of the EUG steel plate along TD. As regards the CG steel plate, toughnesses along ND and TD were measured, respectively. Three V-notch specimens were tested at each temperature in Charpy impact tests. The average value of the three tested results was calculated as the impact absorbed energy at each temperature. The fracture surfaces of the broken impact specimens were observed by a smartphone and a FEI Quanta 600 SEM. The propagation path of the delaminated crack was characterized by the abovementioned ZEISS ULTRA 55 FE-SEM. Cylindrical tensile samples with 8 mm diameter and 70 mm gauge length were machined along RD of the EUG steel plate and CG steel plate according to GB/T 288.1–2010 standard. Tensile tests were conducted using an INSTRON 4206 machine at a constant crosshead speed of 3 mm/min.

3. Results

3.1. Microstructure characters

The SEM observations and EBSD analyses for microstructures of the EUG steel plate and CG steel plate are shown in Fig. 2. As expected, the EUG steel plate has an elongated and ultrafine-grained microstructure because dynamic recovery has been confirmed as the main mechanism during ferrite deformation due to its high stacking fault energy [4,8,12]. The volume fraction of ferrite is 93.6%, and it is 6.4% for pearlite. The perlite was formed by the decomposition of austenite. As regards the CG steel plate, it is the typical polygonal ferrite and pearlite microstructure with volume fractions of 91.6% and 8.4%, respectively, as shown in Fig. 2d.

The result of EBSD analysis in Fig. 2b shows that high-angle grain boundaries (HAGBs) with a fraction of 51.9% are presented in the microstructure of EUG steel plate. The grains with similar orientation distribute in bandings, as shown in Fig. 2c. This is the typical character of EUG microstructures [13,16,17]. As for the CG steel plate, most of

Table 2
Rolling schedule of the EUG steel plate.

Pass	First	Second	Third	Forth	Fifth	Sixth	Seventh	Eighth	Ninth
Thickness/mm	54	44	36	30	26	22	18	15	12
Reduction ratio	16.9%	18.5%	18.2%	16.7%	13.3%	15.4%	18.2%	16.7%	20.0%
Strain rate/s^{-1}	5.6	6.5	7.1	7.4	7.2	8.4	10.0	10.5	12.9

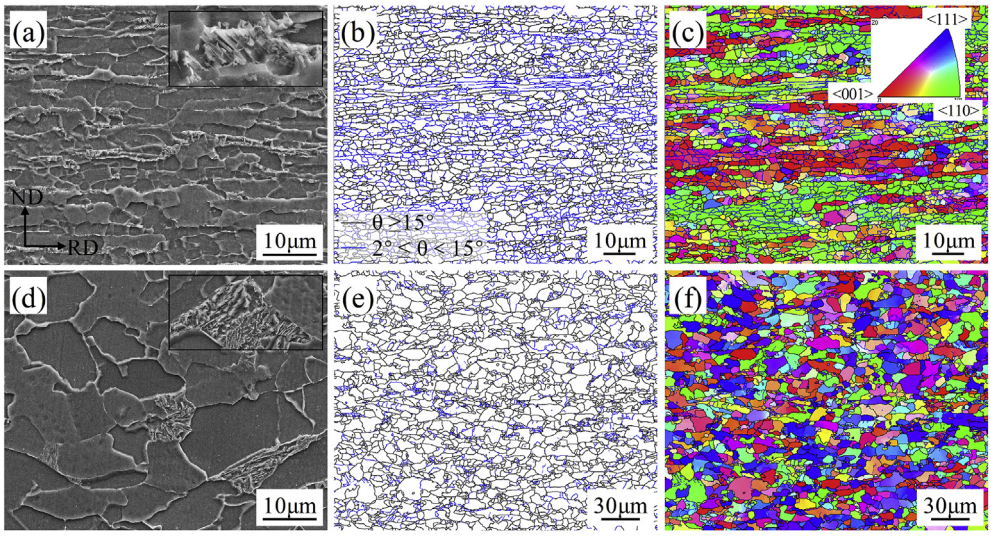

Fig. 2. Microstructures of (a, b, c) EUG steel plate and (d, e, f) CG steel plate. (a) and (d) SEM images, (b) and (e) distributions of grain boundaries, (c) and (f) inverse pole figures.

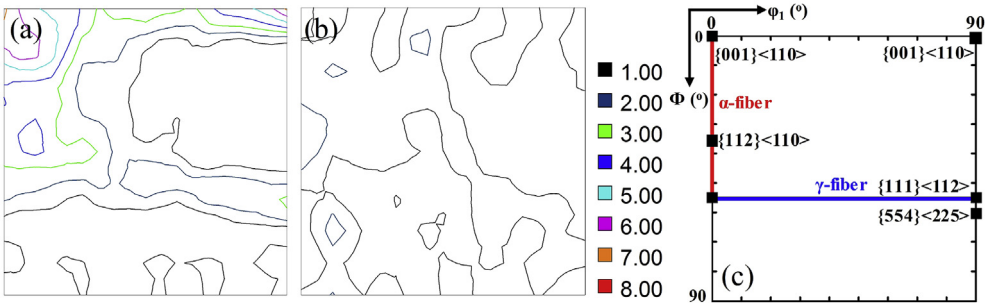

Fig. 3. Crystallographic textures of (a) EUG steel plate, (b) CG steel plate characterized at the cross section of $\phi_2 = 45^\circ$ from the distribution map of orientations and (c) $\phi_2 = 45^\circ$ section of Euler space showing the typical texture components.

the ferrite grains are surrounded by HAGBs. The regions with high density of low-angle grain boundaries (LAGBs) are pearlite colonies, as shown in Fig. 2e. The grains with each orientation distribute uniformly in the microstructure of CG steel plate. The average ferrite grain size of the EUG steel plate is 2.7 μm by calculating the average equivalent circle diameter of grains surrounded by HAGBs. The average ferrite grain size of CG steel plate is 6.4 μm. The crystallographic textures of the EUG steel plate and CG steel plate are shown in Fig. 3. The EUG steel plate has an intense {100} < 011 > texture component and γ-fiber texture component. No obvious texture is found in the CG steel plate.

3.2. Toughness

The results of Charpy impact testing of the EUG steel plate and CG steel plate are shown in Fig. 4. Toughness of the EUG steel plate measured along ND has the highest upper shelf energy. The upper shelf energy is as high as 347 J in the temperature range of 0 °C to −40 °C. When testing temperature is reduced from −40 °C to −60 °C, the absorbed energy is lowered to about 300 J. However, when testing temperature is further dropped to −80 °C, and even to −140 °C, the absorbed energy remains unchanged. Therefore, we can assume that double high upper shelf can exist in the Charpy transition–temperature curve. So the EUG steel plate has excellent low-temperature toughness measured along ND. When testing temperature is reduced to −155 °C, the absorbed energy drops sharply to 181 J. And the absorbed energy further reduces to 13 J at −196 °C, which means the EUG steel plate losses its toughness entirely. On the other hand, high upper shelf energy

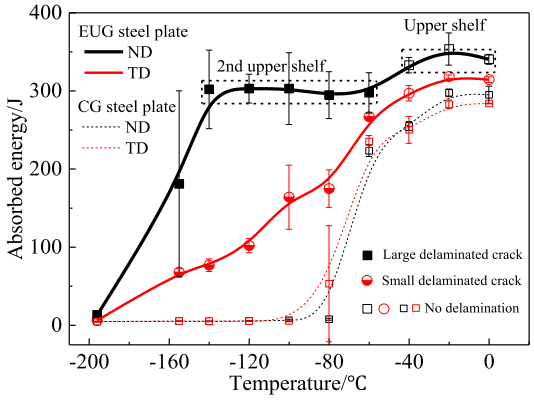

Fig. 4. Charpy transition–temperature curves of EUG steel plate and CG steel plate measured along ND and TD.

is also obtained in the temperature range of 0 °C to −20 °C of the EUG steel plate when toughness is measured along TD. With the decrease in temperature, the absorbed energy reduces at a relatively slow speed. Therefore, high low-temperature toughness is obtained measured along TD of the EUG steel plate.

For the CG steel plate, the toughnesses measured along ND and TD are similar to each other. The upper shelf energies are about 290 J in the temperature range of 0 °C to −20 °C where a ductile fracture behavior is presented (Fig. 5a and Fig. 5d). The absorbed energy decreases rapidly with the decrease in temperature when the temperature falls

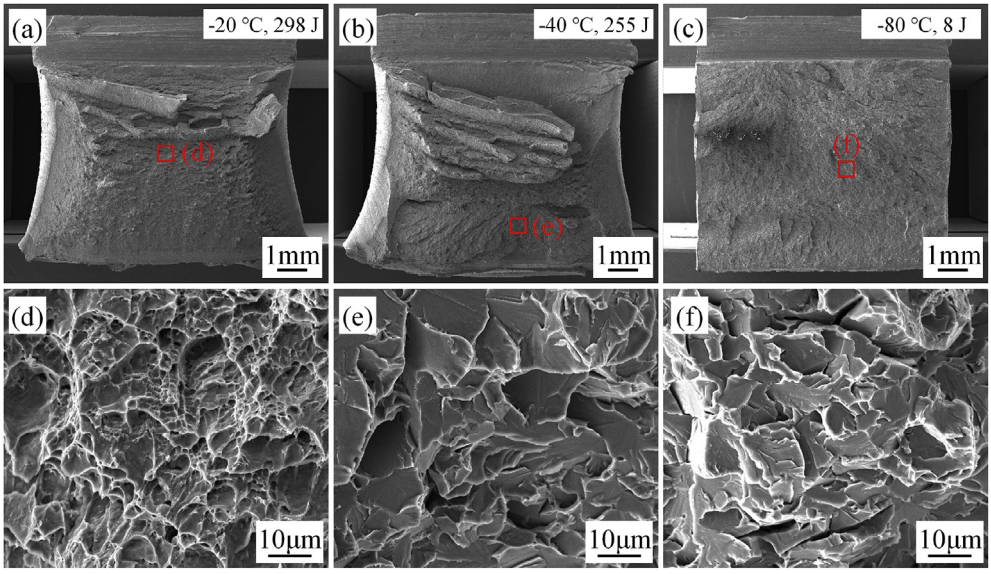

Fig. 5. SEM micrographs of the fracture surfaces of the CG steel plate after Charpy impact tests measured along ND: (a) −20 °C; (b) −40 °C; (c) −80 °C; (d)–(f) enlarged views at particular locations.

below −20 °C. By observing the broken impact specimen, we find this is caused by brittle fracture (Fig. 5b and e). When temperature decreases to −80 °C, fully brittle fracture takes place (Fig. 5c and f). This transition of toughness as a function of temperature is very common in the body-centered cubic (BCC) steels [1,3,12,18]. In the current study, DBTT of the steel plates is determined by the temperature corresponding to the half value of the upper shelf energy. A lowest DBTT is found to be −157 °C for the EUG steel plate when toughness is measured along ND. In addition, the DBTTs of EUG steel plate measured along ND, CG steel plate measured along ND and TD are −102 °C, −67 °C and −70 °C, respectively.

As regards the impact specimens measured toughness for the EUG steel plate along ND, delamination is only presented in the low-temperature region. This phenomenon is also indicated by different symbols in Fig. 4. For the impact specimens measured toughness in the upper shelf region, the fracture surface shows a laminated tearing morphology (Fig. 6a). A large delaminated crack along RD is found when the testing temperature falls below −60 °C (Fig. 6b). The length of delaminated crack increases gradually with the decrease in testing temperature (Fig. 6c and d). At −196 °C, the fracture surface changes a lot and the laminated crack becomes shorter (Fig. 6e). It can be found that the delamination belongs to brittle fracture (Fig. 6f), and the laminated crack propagates through grain boundaries along RD (Fig. 6g). Many micro-cracks with their long axis parallel to RD locate nearby the delaminated crack (Fig. 6g). Meanwhile, there are cementite particles or pearlite colonies in the location of micro-crack. And the ferrite grains are stretched along RD, which means a certain amount of plastic deformation has been happened.

For the impact specimens measured the toughness of the EUG steel plate along TD, it is also fully ductile fracture and no delamination exists in the upper shelf region (0 °C to −40 °C), as shown in Fig. 7a and Fig. 7d. The fracture surface is relatively smooth compared with that measured the toughness of the EUG steel plate along ND. When testing temperature is smaller than −60 °C, delamination starts to appear. For example, three delaminated cracks parallel to rolling plane are found on the fracture surface of specimen tested at −80 °C (Fig. 7b). The

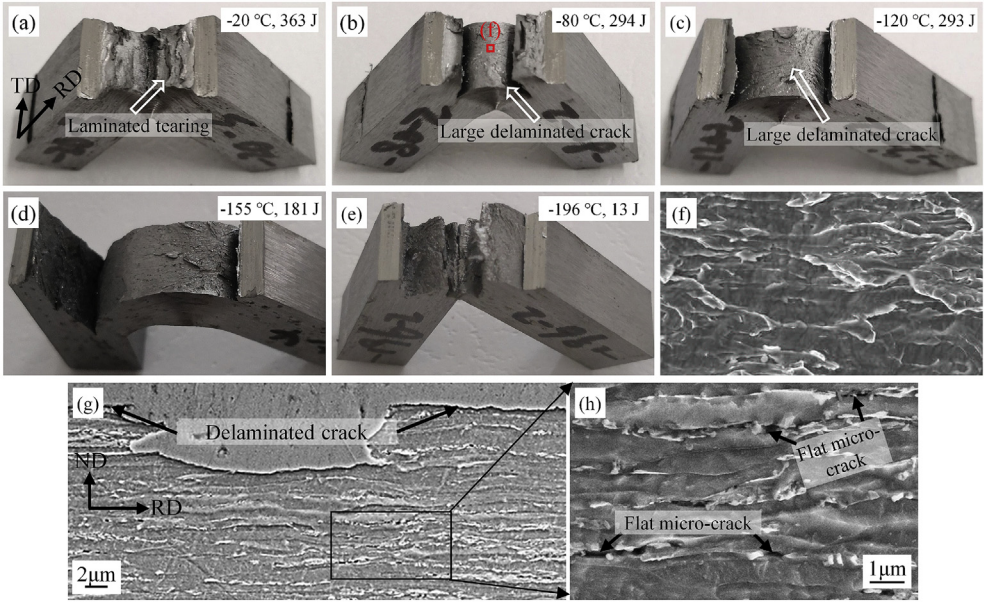

Fig. 6. Fracture surfaces of specimen after the Charpy V-notch impact tests measured the toughness of the EUG steel plate along ND: (a) −20 °C; (b) −80 °C; (c) −120 °C; (d) −155 °C; (e) −196 °C; (f) enlarged view of laminated crack indicated in (b). (g) and (h) microstructure near delaminated crack of specimen tested at −120 °C.

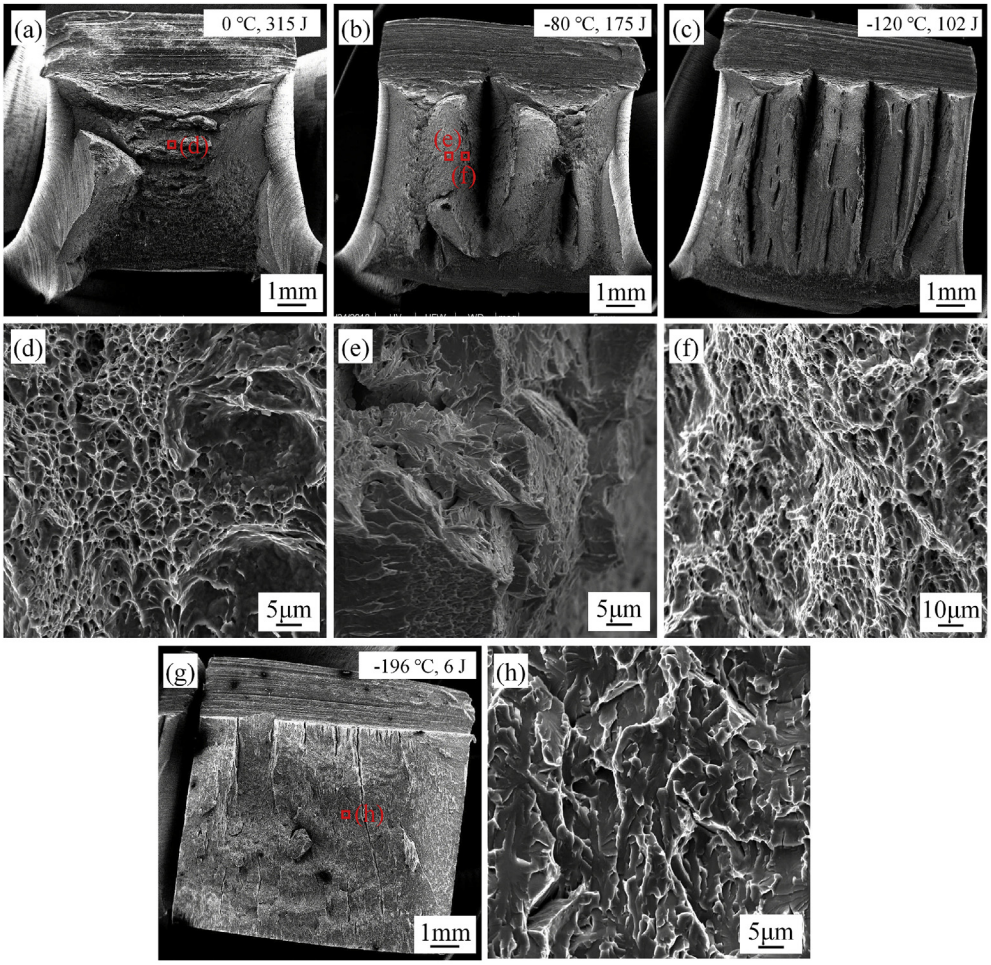

Fig. 7. Fracture surfaces of specimens after the Charpy V-notch impact tests measured the toughness of the EUG steel plate along TD: (a) 0 °C; (b) −80 °C; (c) −120 °C; (d) enlarged view indicated in (a); (e) and (f) enlarged view indicated in (b); (g) −196 °C; (f) enlarged view indicated in (h).

delamination also presented a brittle fracture feature (Fig. 7e), and it is ductile fracture in the area nearby the delaminated crack (Fig. 7f). In the temperature range of −60 °C to −155 °C, delamination is gradually reinforced with the decrease in testing temperature that the number of delaminated cracks increases (Fig. 7c). When the testing temperature decreases to −196 °C, delamination weakens rapidly, and almost completely brittle fracture is presented (Fig. 7g and h).

3.3. Tensile properties

The engineering stress-engineering stress curves of EUG steel plate and CG steel plate are shown in Fig. 8. Unexpectedly, the EUG steel plate possesses a lower strength compared with the CG steel plate. The yield strength of the EUG steel plate (466 ± 3 MPa) is smaller than that of the CG steel plate (483 ± 1 MPa) about 17 MPa. The tensile strength of the EUG steel plate (537 ± 3 MPa) is smaller than that of the CG steel plate (576 ± 3 MPa) 39 MPa. And the total elongations of the EUG steel plate (36.7 ± 1%) is larger than that of the CG steel plate (33.7 ± 0.5%) about 3%.

Generally, steels with ultrafine-grained structure have higher strength than their counterparts with coarse-grained structure due to the strengthening by grain refinement [10,19,20]. However, precipitation strengthening also contributes to the strength of steels. Fig. 9 shows the precipitation particles in the EUG steel plate and CG steel plate. The precipitation particles contain Nb, V and C elements, clarified by energy dispersion spectrum. It can be easily found that the characters of precipitation particles in the two steel plates vary greatly.

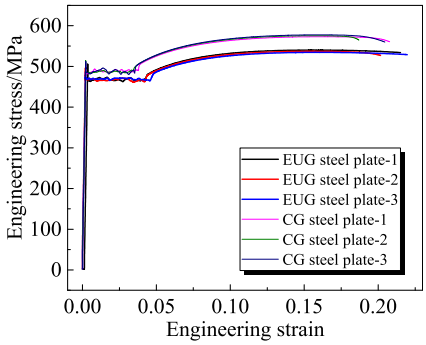

Fig. 8. Engineering stress-engineering strain curves of the EUG steel plate and CG steel plates.

The precipitation particles is coarsen (6.3 ± 1.6 nm) and sparse in the EUG steel plate. But it is fine (4.0 ± 0.9 nm) and dispersive in the CG steel plate. As small-sized and dispersed precipitation particle is beneficial for strength [21,22], we speculate that the above abnormal phenomenon about strength is caused by the different precipitation behavior. In addition, there is a difference in strength between EUG steel plate in our present study and the steel plate that reheating temperature is also 810 °C in our previous study, i.e. 466 MPa vs. 518 MPa. This difference may be caused by diverse dislocation density. Because the EUG steel plate with 12 mm thickness has higher percent of HAGBs than the previous steel plate with 7 mm thickness, i.e. 51.9% vs. 46.8%, which means the lower dislocation density.

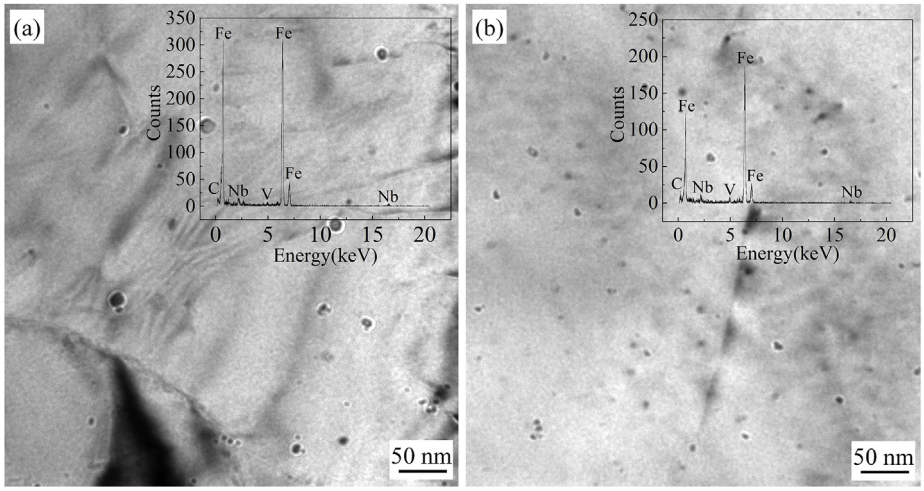

Fig. 9. Precipitation particles in (a) EUG steel plate and (b) CG steel plate observed by TEM.

4. Discussion

4.1. High upper shelf energy

Warm rolling is often used to produce bulk steels with ultrafine-grained microstructure aiming at improving strength and toughness [9,10,16,23]. There are two kinds of warm rolling frequently used. One is flat warm rolling, the other is caliber warm rolling. Generally, flat warm-rolled steels have a low upper shelf energy [9,10]. This phenomenon can be found in the studies of Bourell [9] and Song et al. [10]. Song et al. thought the low upper shelf energy may be caused by low elongation and delamination in the upper shelf region. On the one hand, low elongation means bad plasticity. As a result, the energy absorbed during impact testing is limited. On the other hand, delamination reduces the fraction of ductile fracture on the fracture surface so that less energy is consumed considering that completely ductile fracture will occur if no delamination takes place. Steels generated by caliber warm rolling have high upper shelf energy [8,19,24]. For instance, Inoue et al. found that a caliber warm-rolled steel bar (Fe-0.15C-0.3Si-1.5Mn, mass%) had an upper shelf energy as high as its CG one. Inoue et al. ascribed this high upper shelf energy to relatively high elongation [8].

The flat warm-rolled steel has an elongated and ultrafine-grained microstructure with intense texture containing {100} < 110 > component and γ-fiber ({111}‖ND) component due to the approximately two-dimensional strain state during rolling period [10,12]. The caliber warm-rolled steels has a fibrous and ultrafine-grained microstructure with intense texture containing {100} < 110 > component and {110} < 110 > component due to the three-dimensional strain state during rolling period [8,23]. On the one hand, the microstructure of the flat warm-rolled steel is coarser than caliber warm-rolled one at the same transverse linear interception. On the other hand, the < 110 > ‖RD texture component provides the {110} ductile plane parallel to main fracture surface when toughness is measured along ND or TD, which will promote the motion of dislocation so that the stress at the front of crack is relaxed [19,25]. As a result, plastic deformation is enhanced and more energy is absorbed during impact testing. But only one texture component of the flat warm-rolled steel possesses < 110 > ‖RD texture component compared with the caliber warm-rolled one. Besides, the {110} orientation in the caliber warm rolled steel also favors toughness. Thus, we can get the conclusion that the low upper shelf energy of flat warm-rolled steels may be caused by insufficient refined microstructure and its texture character.

In our present study and previous study, flat rolling was applied in the dual-phase region and an elongated and ultrafine-grained microstructure was also generated. We found no delamination occurred in the upper shelf region. This maybe result from the weakened {100} < 011 > texture component and the reduced degree of laminated microstructure morphology. The effects of reheating temperature on upper shelf energy, yield strength, ferrite grain size and the percent of HAGBs in the EUG steel plates in our previous study are shown in Fig. 10. It can be found that the upper shelf energy increases gradually with the increase in the reheating temperature. When reheating temperature reaches to 810 °C, the upper shelf energy of the EUG steels is first higher than that of the CG one accompanied by the gradually reduce in yield strength from 612 MPa to 518 MPa (Fig. 10a). Increasing reheating temperature results in the increase in the ferrite grain size and the percent of HAGBs, as shown in Fig. 10b. The detail can be found in Ref. [12].

The increase in grain size leads to higher work hardening rate so the

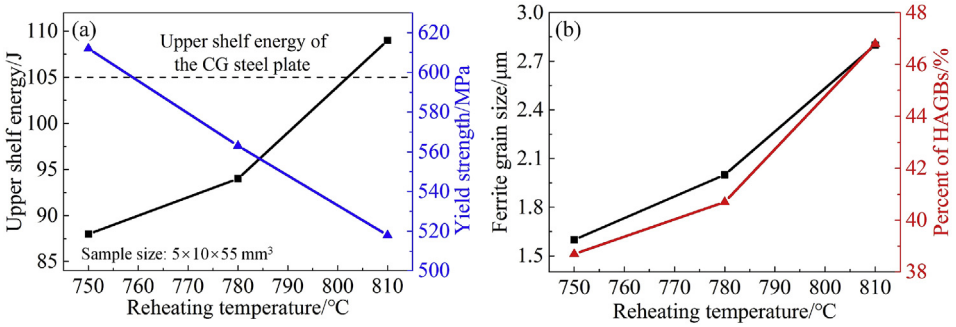

Fig. 10. Effects of reheating temperature on (a) upper shelf energy and yield strength; (b) ferrite grain size and the percent of HAGBs in EUG steel plates in our previous study.

plasticity is improved [10,26]. And the increase in the percent of HAGBs means the reduce in dislocation density, which is favorable for toughness [27,28]. So, we can know that the high upper shelf energy of EUG steels produced by rolling in dual-phase region is caused by relatively coarse grain and low-density dislocation. In the present work, the reheating temperature was chosen as 810 °C to obtain high upper shelf energy according to our previous study. As expected, high elongation and no delamination existed in the upper shelf region are obtained so that high upper shelf energy is gained when toughness is measured along TD. It should be note that the higher upper shelf energy was presented when toughness was measured along ND (Fig. 4). Compared with the corresponding fracture surface of impact samples (Figs. 6a and 7a), we can concern that the laminated tearing ductile fracture is responsible for this higher upper shelf energy, which results from the laminated microstructure morphology.

4.2. Delamination mechanism

Delamination is a typical feature for the fracture surface of laminated composite, caliber/flat warm-rolled steels [7,8,10,13], which is characterized by crack branching normal to the direction of impact load and belongs to brittle crack. The well acceptable elucidation of delamination is the existence of weak interface. The weak interface induces the nucleation of delaminated crack and acts as propagation path for laminated crack. In the laminated composite, the weak interface is heterogeneous boundary between each layer where stress is concentrated during impact period so that delamination is induced. As regards the caliber/flat warm-rolled steels, no heterogeneous boundary exists, the weak interfaces are the boundary of elongated grains with {100} cleavage plane, the interfaces between the ferrite matrix and the cementite colony or aligned cementite particles and two elongated grains with different orientation [8]. Moreover, in the TMCP steel plates, especially pipe steels, delamination also appears on the fracture surface during impact period. Also, the elongated grain with {001} orientation, microstructural banding and banding of the weaker phase (such as thin layers of martensitic or bainitic) are responsible for delamination [29–32]. Furthermore, an important phenomenon is that delamination is dramatically influenced by temperature that delamination trends to appear in the low-temperature region. This phenomenon further concerns that {001} orientation participates in the occurrence of delamination. Because delamination belongs to brittle fracture and {001} orientation plays an important role in brittle fracture varying with temperature of the BCC metals [29,33].

In our present study, microstructure of the EUG steel plate has a banding morphology in which the elongated ferrite grain with {100} orientation layers parallel to the rolling plane (Fig. 2c). Almost all the micro-cracks with a flat shape parallel to rolling plane are nucleated at the location of cementite particle or pearlite colony. Thus, we can conclude that the weak interfaces are elongated ferrite grain boundaries with {100} orientation and the boundaries between ferrite grain and cementite particle or pearlite colony. A particular interface maybe possess the above two characters, which is the weakest interface. Because the BCC metals have ductile-brittle transition phenomenon, delamination with brittle fracture character will occur with the decrease in temperature.

Combining the above theoretical analysis and microstructure observation near the delaminated crack (Fig. 6 g and 6h), delamination mechanism in the present study can be illustrated in Fig. 11. When toughness is measured along ND, the weak interface perpendicular to impact load direction will crack when testing temperature is lower than −60 °C. At the beginning of impacting period, specimen will crack at the V-notch location under the effect of impact load. At the same time, the area beneath the crack tip will take place plastic deformation. Micro-crack will nucleate when the degree of plastic deformation reaches to a certain extent. The elongated microstructure morphology causes the micro-crack with a flat-like shape. As the impacting goes on, micro-crack will grow and coalesce so that delamination is induced and then propagates along the weak interface. Thus, a large delaminated crack is formed. As a result, the main crack changes its original propagation path. With the decrease in testing temperature, the brittleness of weak interface enhances gradually, so the delaminated crack gets longer. However, when testing temperature further reduces to −196 °C, toughness of the EUG steel plate degrades remarkably, which leads to the decrease in delaminated crack.

When toughness is measured along TD, the weak interface will crack when testing temperature is lower than −60 °C. The nucleation, growth and coalescence of micro-crack are as the same as the condition when toughness is measured along ND. However, only small delaminated crack are formed and main crack will not change its propagation path because the weak interface is parallel to the impact load direction. Similarly, delamination is enhanced that the number of delaminated crack increases gradually with the decrease in testing temperature. And delaminated is weakened at −196 °C due to the loss of toughness.

4.3. Delamination toughening

Typically, there are two kinds of delamination. One can change the propagation path of main crack, as shown in Fig. 6 in our present study. The other acts as the branch of main crack, as shown in Fig. 7 in our present study. In terms of the first kind of delamination, toughness is remarkably improved both in upper shelf region and low-temperature region. Because the main crack is blunted obviously so that the specimen becomes a no notch one after delamination. This forceful delamination toughening phenomenon can be found in the studies of Zou et al. [13] and Cao et al. [34]. For instance, the upper shelf energy larger than 450 J and excellent low-temperature toughness (about 105 J at −196 °C) are obtained in a medium-manganese steel plate. As regards the second kind of delamination, some studies indicate that delamination may be responsible for the low upper shelf energy of flat warm-rolled steel plates [10]. But in the low-temperature region, it is confirmed that delamination is helpful for toughness because stress at crack tip is relaxed by delamination.

In our present study, delamination occurs in the low-temperature region. When toughness is measured along ND, the large delaminated crack changes the propagation path of main crack. Therefore, the absorbed energy increases to the extent that the temperature dependence of toughness is changed. Therefore, a second upper shelf appears in the Charpy transition–temperature curve in the temperature range of −60 °C to −140 °C (Fig. 4), and excellent low-temperature is obtained. When toughness is measured along TD, the small delaminated cracks blunt the main crack so that toughness is also improved. Correspondingly, the reducing rate of the absorbed energy with the decrease in temperate is retarded (Fig. 4), and high low-temperature toughness is gained. In addition, it should note that toughness degrades obviously when testing temperature is lower than −140 °C even though large delaminated crack also appears when toughness is measured along ND. This is because the tested microalloyed steel has a BCC crystallographic structure. The BCC steels will become brittle with the decrease in temperature essentially [1,3,12,18]. The measured toughness presented in Fig. 4 indicates that the brittleness of EUG steel is boosted when testing temperature reduces to −155 °C and becomes dominant at −196 °C.

5. Conclusions

A low carbon microalloyed steel plate with a thickness of 12 mm was produced by flat rolling in the dual-phase region. The steel plate had an elongated and ultrafine-grained microstructure and intense {100} < 011 > texture component. The effect of delamination toughening was investigated in detail. The results obtained are as follows.

(1) No delamination appeared in the upper shelf region. When testing

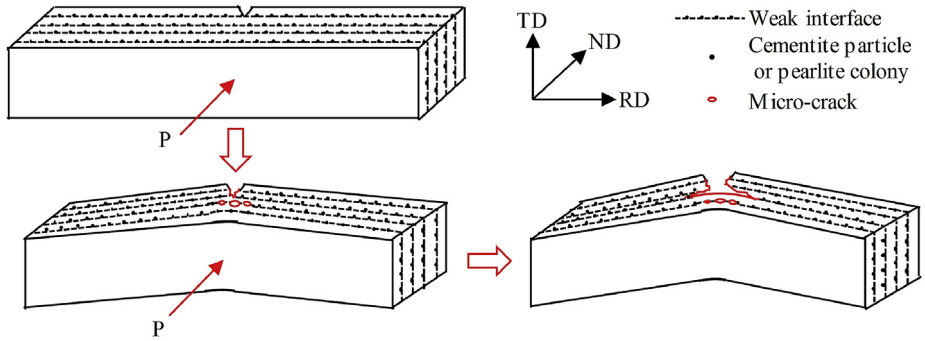

Fig. 11. Schematic diagram of delamination mechanism when toughness is measured along ND. P is the impact load during Charpy impact testing.

temperature was lower than −60 °C, delamination began to take place. A large delaminated crack parallel to rolling plane and propagated along RD was formed in the Charpy impact samples when toughness was measured along ND. Small delaminated cracks were formed on the facture surface of the Charpy impact samples when toughness was measured along TD. The delaminated was caused by the elongated ferrite grains with {100} cleavage plane and the interfaces between ferrite and cementite particle or pearlite colony.

(2) Double upper shelf in the Charpy transition–temperature curve was developed when toughness was measured along ND. The second upper shelf reached up to 300 J in the temperature range from −60 °C to −140 °C, and the DBTT was as low as −157 °C. The second upper shelf was caused by the large delaminated crack, which changed the propagation path of the main crack during impact testing so that the absorbed energy was remarkably improved. High low-temperature toughness was acquired when toughness was measured along TD because of the bluntness of crack tips by the small delaminated cracks.

(3) The developed steel plate had high upper shelf energies when toughnesses were both measured along ND and TD. The high upper shelf energy that toughness was measured along TD resulted from a relatively coarse grain and a high percent of HAGBs. As regards for the higher upper shelf energy that toughness was measured along ND, laminated tearing fracture was a contributor besides the above two factors.

(4) The strength of steel plate with elongated and ultrafine-grained structure was lower than that of steel plate with coarse-grained structure fabricated by TMCP, mainly due to different precipitation features.

Data availability

The raw/processed data required to reproduce these findings cannot be shared at this time as the data forms part of an ongoing study.

Acknowledgements

The supports from National Postdoctoral Program for Innovative Talents (BX201700301), the fundamental researcher funds for the central universities (N170703009) and China Postdoctoral Science Foundation (2018M631803) are gratefully acknowledged. S. Tang thanks the China Scholarship Council (CSC 201706085045) and National Science Foundation of China (51774083) for the financial support.

Appendix A. Supplementary data

Supplementary data to this article can be found online at https://doi.org/10.1016/j.msea.2019.138342.

References

[1] J.W. Morris Jr., Stronger, tougher steels, Science 320 (5879) (2008) 1022–1023, https://doi.org/10.1126/science.1158994.
[2] N. Isasti, D.J. Badiola, M.L. Taheri, P. Uranga, Microstructural features controlling mechanical properties in Nb-Mo microalloyed steels. Part I: yield strength, Metall. Mater. Trans. A 45 (11) (2014) 4960–4971, https://doi.org/10.1007/s11661-014-2450-7.
[3] N. Isasti, D.J. Badiola, M.L. Taheri, P. Uranga, Microstructural features controlling mechanical properties in Nb-Mo microalloyed steels. Part II: impact toughness, Metall. Mater. Trans. A 45 (11) (2014) 4972–4982, https://doi.org/10.1007/s11661-014-2451-6.
[4] R. Song, D. Ponge, D. Raabe, J.G. Speer, D.K. Matlock, Overview of processing, microstructure and mechanical properties of ultrafine grained bcc steels, Mater. Sci. Eng. A 441 (1–2) (2006) 1–17, https://doi.org/10.1016/j.msea.2006.08.095.
[5] J. Chen, M.Y. Lv, S. Tang, Z.Y. Liu, G.D. Wang, Influence of thermomechanical control process on the evolution of austenite grain size, J. Mater. Eng. Perform. 24 (10) (2015) 3852–3861, https://doi.org/10.1007/s11665-015-1700-1.
[6] L. Wang, C.R. Gao, Y.F. Wang, W.Z. Yin, D.W. Zhao, X.H. Liu, Effect of thermo-mechanical controlled processing parameters on microstructure and properties of Q460q steel, J. Iron Steel Res. Int. 17 (1) (2010) 38–43, https://doi.org/10.1016/S1006-706X(10)60042-8.
[7] D.W. Kum, T. Oyama, J. Wadsworth, O.D. Sherby, The impact properties of laminated composites containing ultrahigh carbon (UHC) steels, J. Mech. Phys. Solids 31 (2) (1983) 173–186, https://doi.org/10.1016/0022-5096(83)90049-2.
[8] T. Inoue, F. Yin, Y. Kimura, K. Tsuzaki, S. Ochiai, Delamination effect on impact properties of ultrafine-grained low-carbon steel processed by warm caliber rolling, Metall. Mater. Trans. A 41 (2) (2010) 341–355, https://doi.org/10.1007/s11661-009-0093-x.
[9] D.L. Bourell, Cleavage delamination in impact tested warm-rolled steel, Metall. Trans. A 14 (12) (1983) 2487–2496, https://doi.org/10.1007/BF02668890.
[10] R. Song, D. Ponge, D. Raabe, Mechanical properties of an ultrafine grained C–Mn steel processed by warm deformation and annealing, Acta Mater. 53 (18) (2005) 4881–4892, https://doi.org/10.1016/j.actamat.2005.07.009.
[11] D.B. Santos, R.K. Bruzszek, P.C. M Rodrigues, E.V. Pereloma, Formation of ultrafine ferrite microstructure in warm rolled and annealed C-Mn steel, Mater. Sci. Eng. A 346 (1–2) (2003) 189–195, https://doi.org/10.1016/S0921-5093(02)00519-1.
[12] X.J. Shen, S. Tang, Y.J. Wu, X.L. Yang, J. Chen, Z.Y. Liu, R.D.K. Misra, G.D. Wang, Evolution of microstructure and crystallographic texture of microalloyed steel during warm rolling in dual phase region and their influence on mechanical properties, Mater. Sci. Eng. A 685 (2017) 194–204, https://doi.org/10.1016/j.msea.2016.12.108.
[13] Y. Zou, Y.B. Xu, Z.P. Hu, S.Q. Chen, D.T. Han, R.D.K. Misra, G.Z. Wang, High strength-toughness combination of a low-carbon medium-manganese steel plate with laminated microstructure and retained austenite, Mater. Sci. Eng. A 707 (2017) 270–279, https://doi.org/10.1016/j.msea.2017.09.059.
[14] M.D. Zhang, J. Hu, W.Q. Cao, H. Dong, Microstructure and mechanical properties of high strength and high toughness micro-laminated dual phase steels, Mater. Sci. Eng. A 618 (2014) 168–175, https://doi.org/10.1016/j.msea.2014.08.073.
[15] M.D. Zhang, J. Hu, W.Q. Cao, H. Dong, Microlaminated dual phase steel presenting with high strength and ultrahigh toughness, Mater. Sci. Technol. 31 (11) (2014) 1349–1354, https://doi.org/10.1179/1743284714Y.0000000699.
[16] R. Song, D. Ponge, D. Raabe, R. Kaspar, Microstructure and crystallographic texture of an ultrafine grained C–Mn steel and their evolution during warm deformation and annealing, Acta Mater. 53 (18) (2005) 845–858, https://doi.org/10.1016/j.actamat.2004.10.051.
[17] B. Eghbali, EBSD study on the formation of fine ferrite grains in plain carbon steel during warm deformation, Mater. Lett. 61 (18) (2007) 4006–4010, https://doi.org/10.1016/j.matlet.2007.01.019.
[18] X.J. Shen, S. Tang, J. Chen, Z.Y. Liu, G.D. Wang, Improving toughness of heavy steel plate by deformation distribution under low finish cooling temperature, J. Mater. Eng. Perform. 25 (9) (2016) 3682–3690, https://doi.org/10.1007/s11665-016-2210-5.
[19] M. Song, C. Sun, Y.X. Chen, Z.X. Shang, J. Li, Z. Fan, K.T. Hartwig, X.H. Zhang, Grain refinement mechanisms and strength-hardness correlation of ultra-fine grained grade 91 steel processed by equal channel angular extrusion, Int. J. Press.

Vessel. Pip. 172 (2019) 212–219, https://doi.org/10.1016/j.ijpvp.2019.03.025.
[20] S.L. Gibbons, R.A. Abrahams, M.W. Vaughan, R.E. Barber, R.C. Harris, R. Arroyave, I. Karaman, Microstructural refinement in an ultra-high strength martensitic steel via equal channel angular pressing, Mater. Sci. Eng. A 725 (2018) 57–64, https://doi.org/10.1016/j.msea.2018.04.005.
[21] N. Gao, D.H. Lu, Y.Y. Zhao, X.W. Liu, G.H. Liu, Y. Wu, G. Liu, Z.T. Fan, Z.P. Lu, E.P. Grorge, Strengthening of a CrMnFeCoNi high-entropy alloy by carbide precipitation, J. Alloy. Comp. 792 (2019) 1028–1035, https://doi.org/10.1016/j.jallcom.2019.04.121.
[22] S.H. Jiang, H. Wang, Y. Wu, X.J. Liu, H.H. Chen, M.J. Yao, B. Gault, D. Ponge, D. Raabe, A. Hirata, M.W. Chen, Y.D. Wang, Z.P. Lu, Ultrastrong steel via minimal lattice misfit and high-density nanoprecipitation, Nature 544 (7651) (2017) 460–464, https://doi.org/10.1038/nature22032.
[23] Y. Kimura, T. Inoue, F.X. Yin, K. Tsuzaki, Inverse temperature dependence of toughness in an ultrafine grain-structure steel, Science 320 (5879) (2008) 1057–1060, https://doi.org/10.1126/science.1156084.
[24] M. Jafari, Y. Kimura, K. Tsuzaki, Enhancement of upper shelf energy through delamination fracture in 0.05 pct P doped high-strength steel, Metall. Mater. Trans. A 43 (7) (2012) 2453–2465, https://doi.org/10.1007/s11661-012-1095-7.
[25] J. Kang, C.N. Li, G. Yuan, G.D. Wang, Improvement of strength and toughness for hot rolled low-carbon bainitic steel via grain refinement and crystallographic texture, Mater. Lett. 175 (2016) 157–160, https://doi.org/10.1016/j.matlet.2016.04.007.
[26] O. Saray, G. Purcek, I. Karaman, H.J. Maier, Impact toughness of ultrafine-grained interstitial-free steel, Metall. Mater. Trans. A 43 (11) (2012) 4320–4330, https://doi.org/10.1007/s11661-012-1238-x.
[27] C.N. Li, G. Yuan, F.Q. Ji, D.S. Ren, G.D. Wang, Effects of auto-tempering on microstructure and mechanical properties in hot rolled plain C-Mn dual phase steels, Mater. Sci. Eng. A 665 (2016) 98–107, https://doi.org/10.1016/j.msea.2016.04.038.
[28] B. Jiang, M. Wu, M. Zhang, F. Zhao, Z.G. Zhao, Y.Z. Liu, Microstructural characterization, strengthening and toughening mechanisms of a quenched and tempered steel: effect of heat treatment parameters, Mater. Sci. Eng. A 707 (2017) 306–314, https://doi.org/10.1016/j.msea.2017.09.062.
[29] A. Gervasyev, R. Petrov, L. Pyshmintsev, A. Struin, B. Leis, Mechanical properties anisotropy in X80 line pipes, Proceedings of the 2016 11th International Pipeline Conference, IPC2016, Calgary, Alberta, Canada, 2016, pp. 1–7.
[30] A. Gervasyev, V.C. Olalla, J. Sidor, N.S. Mouriño, L.A.I. Kestens, R.H. Petrov, An approach to microstructure quantification in terms of impact properties of HSLA pipeline steels, Mater. Sci. Eng. A 677 (2016) 163–170, https://doi.org/10.1016/j.msea.2016.09.043.
[31] L. Pyshmintsev, A. Gervasyev, R.H. Petrov, V.C. Olalla, L. Kestens, Crystallographic texture as a factor enabling ductile fracture arrest in high strength pipeline steel, Mater. Sci. Forum 702–703 (2011) 770–773 https://doi.org/10.4028/www.scientific.net/MSF.702-703.770.
[32] M.S. Joo, D.W. Suh, J.H. Bae, H.K.D.H. Bhadeshia, Role of delamination and crystallography on anisotropy of Charpy toughness in API-X80 steel, Mater. Sci. Eng. A 546 (2012) 314–322, https://doi.org/10.1016/j.msea.2012.03.079.
[33] H.K.D.H. Bhadeshia, S.R. Honeycombe, Steels: Microstructure and Properties, third ed., Cambridge University, UK, 2006, pp. 235–236.
[34] W.Q. Cao, M.D. Zhang, C.X. Huang, S.Y. Xiao, H. Dong, Y.Q. Weng, Ultrahigh Charpy impact toughness (~450J) achieved in high strength ferrite/martensite laminated steels, Sci. Rep. 7 (2017) 1–8, https://doi.org/10.1038/srep41459.